Nucleation of vacancy precipitation during quenching of metals

Jane Wiberg and Olof Vingsbo
Uppsala University, Institute of Technology, Box 534, S-751 21 Uppsala, Sweden
(Received 4 September 1975; revised manuscript received 20 October 1976)

A theoretical model describing the nucleation of vacancy precipitation in pure metals is investigated. The model introduces a new definition of nucleation based on a change in conditions from random walk to concentration-gradient-controlled vacancy diffusion. Monovacancy as well as divacancy diffusion is considered. Vacancy cluster concentrations are computed as functions of temperature during quenching for clusters of up to six vacancies. The critical temperatures T^* for nucleation of precipitation are computed for all considered cluster sizes. Numerical parameter values are chosen to represent aluminium. The obtained densities of vacancy precipitation nuclei are compared with available literature values of dislocation-loop densities in quenched aluminium. Within the investigated limits, the choice of maximum cluster size before nucleation of precipitation is not critical for the resulting densities of nuclei and nucleation temperatures T^*.

I. INTRODUCTION

Clustering and precipitation of vacancies is a phenomenon which is interesting from thermodynamical as well as mechanical points of view for many metals. A great number of quenching and annealing experiments have been reported in the literature, using calorimetric, resistivity, and density measurements, as well as structural studies by transmission electron microscopy.

Initially, quenching was considered as an instantaneous event, and all vacancy clustering was assumed to take place during subsequent annealing (see, e.g., Refs. 1 and 2). Later, however, the possibility of cluster formation and growth during the actual quench was considered by Cotterill,[3] Kuhlman-Wilsdorf,[4] and Doyama.[5]

Silcox and Whelan[6] have used a "continuum" approach to examine the special case of growth of prismatic dislocation loops at constant temperature. Their expression can be generalized for the case of voids. Wiberg *et al.*[7] used a similar method to describe growth of voids during quenching of aluminum. However, a continuum model must be based on an assumption of preexisting vacancy precipitation nuclei, and cannot describe the early stages of a quench, when the vacancy clusters form and break up by random processes. For this purpose an "atomistic" approach is necessary.

Cotterill[3] used the atomistic approach in a qualitative theoretical study of vacancy clustering during a quench. He obtained the principal behavior of the concentration versus time curves, when clusters of up to four vacancies compete in the presence of low contents of impurity atoms. He concluded that there was no unifying theory capable of explaining all observations in quenching experiments.

In the present work, an atomistic approach is again used to describe vacancy clustering during a quench and special attention is paid to the nucleation mechanism. A new concept is suggested for the definition of nucleation in terms of a change in diffusion conditions.

II. VACANCY CLUSTERING DURING RANDOM-WALK DIFFUSION

Irrespective of equilibrium conditions, the formation, growth, and breakup of vacancy clusters can be described by random-walk diffusion of vacancies at sufficiently high temperatures. In most metals, the migration enthalpy of mono and divacancies is so much lower than that of large clusters that it is not necessary to consider more than mono and divacancy diffusion. Larger clusters are essentially immobile during their lifetime, but change sizes continually by absorbing or emitting mono or divacancies. (In this respect, the instantaneous position of, for instance, all tetravacancies changes with time.)

The random-growth and breakup process of vacancy clusters is described according to Fig. 1. Clusters v_i ($i \geq 3$ is the number of empty lattice sites momentarily constituting the cluster) occur at a concentration c_i within an atmosphere of migrating (diffusing) mono and divacancies v_j of concentrations c_j, $j = 1, 2$. α_{ji} are probability coefficients for the transition of a v_{i-j} to a v_i by association with a v_j, while α_{ij} refers to the dissociation of a v_i to a v_{i-j} plus a v_j. All interaction between more than two units (e.g., the association of three monovacancies to a trivacancy) is neglected. Furthermore, if all vacancy sinks but clusters are neglected,

$$\sum_i i c_i(t) = \text{const} \tag{1}$$

and

$$\sum_i \frac{dc_i}{dt} = 0 . \tag{2}$$

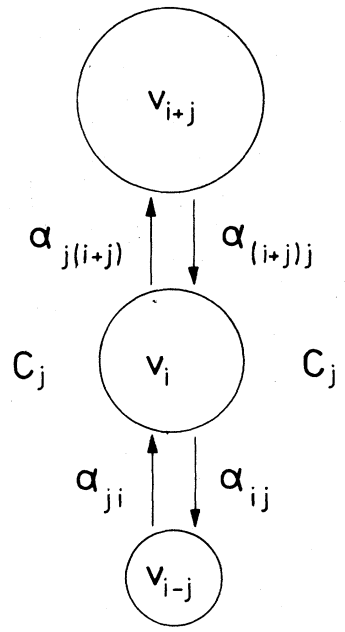

FIG. 1. Growth and breakup of vacancy clusters by random-walk diffusion. v_i is a cluster of i monovacancies ($i \geq 3$) in an atmosphere of migrating units v_j ($j = 1, 2$). Growth (upward arrows) takes place by association and consumes a v_j. Breakup (downward arrows) corresponds to dissociation, creating a v_j.

Developing the ideas of Cotterill,[3] Doyama,[5] or Koehler *et al.*,[8] the association and dissociation rates can be expressed by a system of differential equations in dc_i/dt. The general rate equation is

$$\frac{dc_i}{dt} = \sum_{j=1}^{2} \alpha_{ji} c_j c_{i-j} + \alpha_{(i+j)j} c_{i+j} - c_i(\alpha_{ij} + \alpha_{j(i+j)} c_j); \quad i \geq 3, \tag{3}$$

$$\alpha_{23} = \alpha_{32} = 0. \tag{4}$$

The corresponding rate equation for the migrating v_j configurations is

$$\frac{dc_j}{dt} = (j-1)(\alpha_{1j} c_1^2 - \alpha_{j1} c_j) + \alpha_{2j,j} c_{2j} - \alpha_{j,2j} c_j^2 + \sum_{i=j+1}^{n} (\alpha_{ij} c_i - \alpha_{ji} c_j c_{i-j}); \quad j = 1, 2, \tag{5}$$

where also interaction between mono and divacancies has been taken into account in the terms outside the summation. Conditions (4) simply reflect the fact that, with the present indexing, the transitions α_{23} and α_{32} are equivalent to transitions α_{13} and α_{31}, respectively.

The probability coefficients are

$$\alpha_{ji} = G_{ji} \nu e^{-M_j/kT} \tag{6}$$

for association, and

$$\alpha_{ij} = G_{ij} \nu e^{-(M_j + B_{ij})/kT} \tag{7}$$

for dissociation. G is a geometrical factor, ν is the atomic vibration frequency, M_j is the migration enthalpy for v_j, and B_{ij} is the binding enthalpy of a v_j in a v_i cluster. ν is the product of the Debye frequency ν_0 and an entropy factor $e^{\Delta S/k}$. The entropy has, however, been neglected, and the approximation $\nu = \nu_0$ is used. G is calculated as the number of geometrically possible jumps for the event in question, and depends on the configuration of any any particular cluster. It has been tabulated for $i = 3$ for all possible shapes of trivacancies in an fcc lattice by Koehler *et al.*[8] Already, for $i = 4$, however, the number of different geometries, each representing its own contribution to the total concentration C_4, constitutes an extensive problem. Compared to the exponential factors in Eqs. (6) and (7), and the c_i values in Eqs. (3) and (5), the influence of G rapidly falls with i, and the following simplification has therefore been used in the present calculations.

The rearrangement from one configuration (a) to another (b), with constant i is controlled by a probability coefficient

$$\alpha_{ab} = G_{ab} \nu e^{\Delta B_{ab}/kT}, \tag{8}$$

where ΔB_{ab} is the (unknown) difference in binding enthalpy between the two configurations.

$|\Delta B_{ab}|$ is a small quantity compared to M_j and B_{ij}, and at the high temperatures which are considered, a cluster is continually and rapidly swinging between its different geometries. The cross-section area for collision with a v_j then approximates that of a sphere of radius

$$R_i = \tfrac{1}{2} b i^{1/3} \tag{9}$$

(b is the shortest interatomic distance). G is now considered proportional to the sphere surface, and is approximated by

$$G_i = G_{i-1}[i/(i-1)]^{2/3} \tag{10}$$

for $i > 3$, $j = 1$ and for $i > 4$, $j = 2$. The corresponding values are given in Table I.

The binding enthalpies B_{ij} approach the mono and divacancy formation enthalpies F_j for increas-

TABLE I. Applied approximations for the geometrical probability factor G and the binding enthalpies of mono and divacancies to vacancy clusters.

i	G_i	B_{i1}	B_{i2}
2		$0.25F_1$	
3		$0.45F_1$	$0.64F_1$
4	$1.22G_3$	$0.56F_1$	$0.87F_1$
5	$1.16G_4$	$0.64F_1$	$1.03F_1$
6	$1.14G_5$	$0.70F_1$	$1.14F_1$

ing i, and are assumed to obey the empirical relation

$$B_{i1} = F_1[(i-1)/i]^2 , \tag{11}$$

$$B_{i2} = 2B_{i1} - B_{21} = F_1\{2[(i-1)/i]^2 - \tfrac{1}{4}\} , \tag{12}$$

which is in agreement with numerical estimates by Cotterill.[3] The applied approximations are given in Table I.

III. QUENCHING CONDITIONS

The system of rate equations (3)–(5) describes the variation of c_i with time. A quench is described by the relevant temperature-time relationship, with the aid of which the time derivatives can be transformed to temperature derivatives. The solution of (3)–(5) then gives the actual concentrations $c_i = c_i(T)$ during the quench.

In the present investigation the conditions were chosen so as to correspond to a water quench according to Hellström *et al*,[9] and may be described by the exponential relation

$$T = T_0 + (T_q - T_0)e^{-\Theta t} , \tag{13}$$

where the coefficient Θ determines the quenching rate.

IV. NUCLEATION OF VACANCY PRECIPITATES

As seen from Eq. (7), the dissociation probability coefficient α_{ij} can be considered as the frequency of successful attempts to break up a v_i cluster. The corresponding average lifetime

$$\tau_{ij} = (\alpha_{ij})^{-1} , \tag{14}$$

often referred to as the breakup time, is then a function of temperature, according to

$$\tau_{ij} = (\nu_0 G_{ij})^{-1} e^{(M_j + B_{ij})/kT} . \tag{15}$$

With the same indexing as for α, the mean free path of a migrating v_j for collision with v_i cluster is defined by

$$x_{ij} = [i/(N_0 c_i)]^{1/3} , \tag{16}$$

where N_0 is the number of lattice points per unit volume.

Einstein's formula gives the corresponding average migration time

$$t_{ij} = (\tfrac{1}{2}x_{ij}/2D_j)^2 , \tag{17}$$

where

$$D_j = D_0 e^{-M_j/kT + \Delta S/k} \simeq a^2 \nu_0 e^{-M_j/kT} \tag{18}$$

is the diffusion coefficient for a v_j (a is the lattice parameter). It is now possible to express the migration time as a function of temperature as follows.

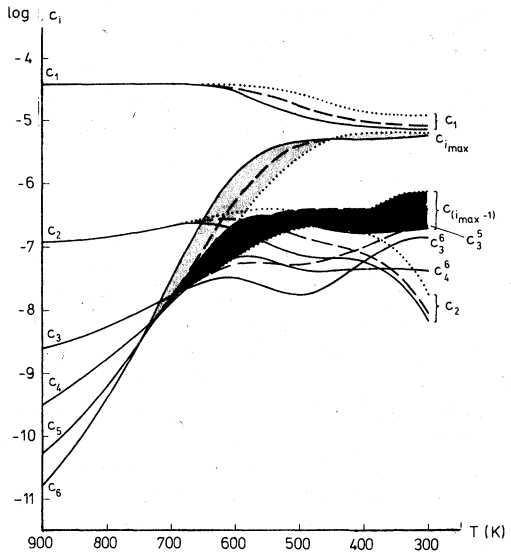

FIG. 2. $c_i(T)$ curves for $i_{max} = 6$ (full lines), $i_{max} = 5$ (dashed lines), and $i_{max} = 4$ (dotted lines). The c_i superscripts, when applied, refer to i_{max}. ($F_1 = 0.76$ eV, $M_1 = 0.75$ eV, and $M_2 = 0.50$ eV.)

$$t_{ij}(T) = x^2_{ij}/8D_j = (e^{M_j/kT} i^{2/3}/8a^2\nu_0 N_0^{2/3}) c_i^{-2/3} , \tag{19}$$

where $c_i = c_i(T)$ is the solution of the rate equations (3)–(5). It will be shown later (see Fig. 2) that all c_i, $i > 2$, increase rapidly at the beginning of a quench, with the consequence that both τ_{ij} and t_{ij} decrease. A numerical comparison shows that, for sufficiently high temperatures at the beginning of the quench, $\tau_{ij} < t_{ij}$, and both association and dissociation take place by random walk diffusion as described by Eqs. (3)–(5).

Below a critical temperature $T_{ij} = T^*_{ij}$, however, the breakup time is longer than the migration time, and vacancies begin to flow into the v_i cluster. This implies the development of vacancy concentration gradients around the cluster, which at the same time becomes localized in space and starts to grow.

The change from random-walk to gradient-controlled vacancy diffusion is hereby introduced as a definition of the nucleation of a vacancy precipitate. The critical temperature T^*_{ij}, typical of each particular ij combination, is obtained from the critical condition

$$\tau_{ij} = t_{ij} . \tag{20}$$

After substitution of Eqs. (15) and (19), T^*_{ij} is implicitly given by

$$T^*_{ij} = (B_{ij}/k)[\ln G_{ij} - \ln 8a^2 - \tfrac{2}{3}\ln(N_0/i) - \tfrac{2}{3}\ln c_i(T^*_{ij})]^{-1} . \tag{21}$$

This equation can be solved numerically, or graphically from the intersection of the $t_{ij}(T)$ and $\tau_{ij}(T)$ curves.

The present definition of T^* can be compared with earlier suggestions and calculational methods, e.g., in Ref. 3.

V. NUMERICAL COMPUTATION

The rate equations (3)–(5) and the nucleation temperatures T^*_{ij} have been solved numerically for $i \leq 6$ with the aid of an IBM 370/155 digital computer. The digital solution of up to six coupled differential equations represents a rather difficult problem, particularly as the range of c_i spans over many orders of magnitude, and the derivatives dc_i/dt are differences between terms, each of which is many orders of magnitude larger than dc_i/dt itself.

Numerical values were chosen to represent aluminium. The only boundary condition necessary is Eq. (1).

VI. RESULTS AND DISCUSSION

A. General properties of the concentration curves

The essential parameters of the model have been varied in order to study the effects on the family of $c_i(T)$ curves, and on the nucleation temperatures T^*_{ij}. Irrespective of the choice of parameter values, the principal shape and position of the curves was always the same, as seen from the diagrams in Figs. 2–4.

Because there is a finite binding energy of a migrating unit to a cluster, there is a higher probability of association than dissociation, and all cluster concentrations grow with decreasing temperature at the expense of the monovacancies. After $T = 600$ K, clusters of all orders except i_{max} occur in roughly the same concentrations (about 10^{-7}). Mutual competition then causes irregular curve shapes, the detailed interpretation of which is not of interest for the present model. The only significant feature is a continuous loss of divacancies in this interval.

B. Quench parameters

The quench temperature Tq was kept constant, in order to allow assumption of a high initial vacancy content.

The quench rate was altered by varying the time coefficient θ and the temperature T_0 of the cooling medium in the intervals

$$7 \leq \theta \leq 30, \quad 85 \leq T_0 \leq 285 \text{ K}.$$

Only minor differences were obtained in the curve tails, for $T < 400$ K, and in all the runs reported, the values $\theta = 7$ and $T_0 = 285$ K were chosen as best representing a water quench.

TABLE II. Applied basic G values.

i	Cluster geometry	G_{1i}	G_{i1}	G_{2i}	G_{i2}
2		84	14		
3	60°	20	15		
	90°	24			
	120°	56			
	180°	14			
4				56	4

C. Geometry factor G_{ij}

As seen from Eq. (10) and Table I, the approximated G_{ij} values are based on G_{13} and G_{31} for monovacancy diffusion, and by G_{24} and G_{42} for divacancy diffusion. Table II gives the applied values. G_{13} was varied for all possible geometries, including different sums up to $G_{13} = 114$.

The lowest G_{13} values resulted in a somewhat lower consumption of the migrating units and a correspondingly reduced c_i growth rate for $i \geq 3$. No essential relative changes occurred, however, and in all the reported examples, the value $G_{13} = 114$ has been used.

D. Maximum cluster size

The maximum size of clusters, considered during the random walk diffusion, is given by the choice i_{max} of maximum cluster order. A basic problem is to what extent this restriction affects the validity of the model. Naturally, because the initial cluster concentrations $c_{ij}(Tq)$ decrease with increasing size, very big clusters must be negligibly few. Mainly for computational reasons, the present calculations have been restricted to $i_{max} \leq 6$.

As mentioned in Sec. VI A, all c_i for $i > 1$ are expected to, and also found to, increase during the quench. The fact that the binding enthalpies increase with i implies that the rate of concentration increase is always higher for bigger clusters, which is also seen from the diagrams for $T > 600$ K. In addition, however, c_{imax} always exceeds all concentrations of smaller clusters and approaches $c_1 \lesssim 10^{-5}$ for $T < 450$ K, irrespective of the choice of i_{max}. An example ($i_{max} = 4, 5, 6$) is reproduced in Fig. 2, which also shows that the three c_{imax} curves are essentially the same. This property of the model is of central importance, particularly with regard to the nucleation conditions, and will be discussed later in Sec. VI H.

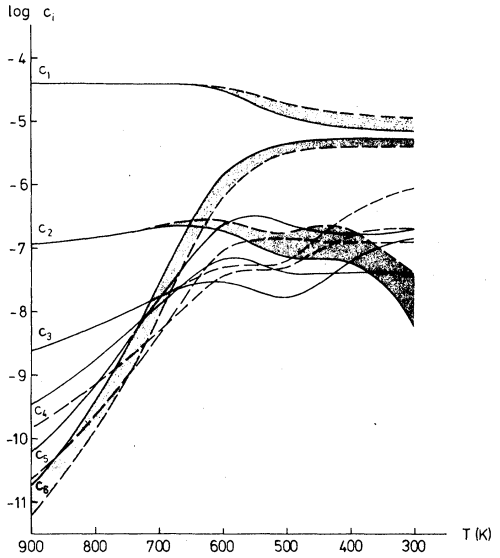

FIG. 3. Effect of divacancy diffusion. The case of both mono and divacancies as migrating units (full lines) is compared to the case of neglecting all association with divacancies (dashed lines). ($i_{max}=6$, $F_1=0.76$ eV, $M_1=0.75$ eV, and $M_2=0.50$ eV.)

E. Mono and divacancy diffusion

The influence of divacancy diffusion was studied by eliminating all divacancy association. (This was simply achieved by choosing $G_{24}=0$, which gives all divacancy association probability coefficients $\alpha_{2i}=0$.)

The effect is not drastic, as demonstrated by the two families of curves in Fig. 3. Naturally, the divacancy concentration increases, but the general c_2 drop for the lowest temperatures is still visible. At the same time, however, the monovacancy losses decreased, primarily at the expense of $c_{i\max}$, which is of greater importance for the prediction of vacancy precipitation densities. Therefore, divacancy migration is always included in the results reported hereafter.

The effect of neglecting divacancy dissociation ($G_{42}=0$) was minimal, which simply reflects the high binding energies of divacancies.

F. Vacancy formation and migration enthalpies

Because the binding enthalpies are expressed in the monovacancy formation enthalpy F_1 the latter has a rather strong influence via the exponential relationships (6) and (7). F_1 was varied slightly, between the literature values 0.73 (Ref. 10) and 0.76 eV,[1] typical of aluminium, with the resulting curve shifts of Fig. 4.

Although exaggerated by the logarithmic scale in Fig. 4, the effect may be of importance in the interesting temperature range $T \geq 600$ K (cf. Sec. VIG).

The monovacancy migration enthalpy M_1 was varied between the limits of 0.62 (Ref.1) and 0.75 eV.[10] The effect was much lower than that of varying F_1, and can be neglected together with the even smaller effect of varying M_2.

G. Nucleation conditions

Critical temperatures T^*_{ij} for defining the nucleation conditions of vacancy precipitation, were numerically computed according to Eq. (21). A summary of representative (c_i, T^*_{ij}) coordinates are plotted in the c_i-T surface of Fig. 5(a) for $i_{max}=6$.

The points corresponding to $j=2$ are well grouped along the early steep part of the c_i curves. The chronology is always such that bigger clusters of correspondingly lower concentrations nucleate first.

For monovacancy diffusion, the biggest clusters again nucleate first, but now occur at the highest concentrations. All the smaller clusters nucleate later, in the range where the irregularity of the concentration curves affects the exact coordinates.

The divacancy-controlled nucleation is thus found to occur first (at the highest temperature). It is, however, numerically negligible, because the resulting concentration of precipitation nuclei (about 10^{-8}) is two orders of magnitude lower than that corresponding to monovacancy controlled nucleation (about 10^{-6}).

If, consequently, the nucleation at $T^*_{i\max 2}$ is dis-

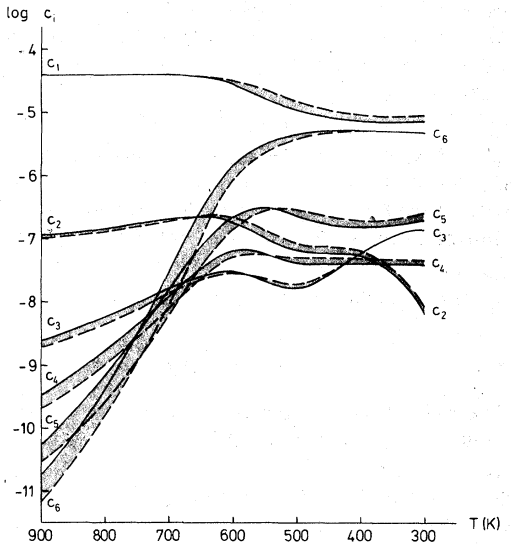

FIG. 4. Effect of varying the monovacancy formation enthalpy from 0.73 (dashed lines) to 0.76 eV (full lines). ($i_{max}=6$, $M_1=0.75$ eV, and $M_2=0.50$ eV.)

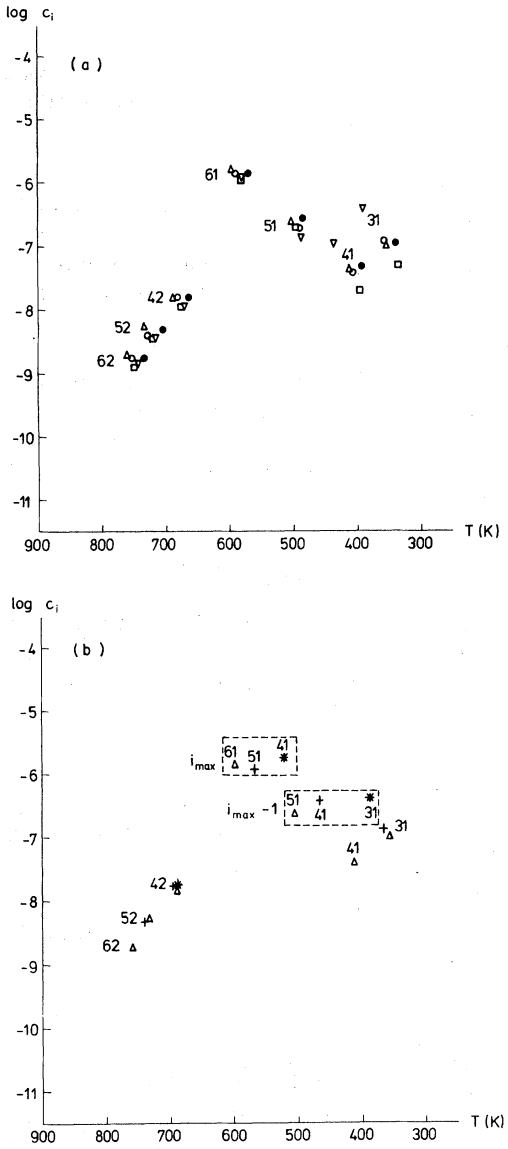

FIG. 5. Vacancy precipitation nucleation coordinates (c_i, T^*_{ij}) for some representative parameter sets. The numbers in the diagrams refer to the i and j subscripts, respectively.

(a) $i_{max} = 6$

	F_1 (eV)	M_1 (eV)	M_2 (eV)	
Δ	0.76	0.75	0.50	
∇	0.76	0.75	0.50	(no divacancy association)
□	0.76	0.62	0.62	
○	0.76	0.68	0.50	
●	0.73	0.75	0.50	

(b) $F_1 = 0.76$ eV, $M_1 = 0.75$ eV, and $M_2 = 0.50$ eV.

	i_{max}
Δ	6
+	5
*	4

regarded, and T^*_{imax1} is considered to represent the physically effective nucleation temperatures, it is possible to judge to what extent the unavoidable choice of i_{max} affects the results of the model.

Figure 5(b) demonstrates the effect of varying i_{max} between 4 and 6. It is seen that the three T^*_{imax1} nucleation points [the upper box in Fig. 5(b), with indices 61, 51, and 41] form a very narrow group in the diagram. The corresponding concentration of nuclei is about 10^{-6} *irrespective of the choice of* i_{max}.

Also, the $i = i_{max-1}$ points, though at lower concentrations, form a well-defined group which, however, modelwise cannot contribute. Once nucleation has occurred, the present definition of nucleation as a transition from random-walk to gradient-controlled diffusion makes the rate equations (3)–(5) irrelevant for describing events at temperatures $T < T^*$, and all corresponding $c_i(T < T^*)$ curve tails must be disregarded. The i_{max} clusters now define the positions of the nuclei and grow by monovacancy diffusion in the established vacancy concentration gradients. The continued growth of vacancy precipitates proceeds during the quench process according to mechanisms described previously,[7] and will not be further treated here.

H. Applicability of the model

It has thus been shown that the suggested model describes the temperature dependence of the cluster concentrations $c_{i,max}(T)$ before nucleation essentially independently of the choice of i_{max}. Above all, however, the obtained concentration $c_{imax}(T^*_{imax1})$ of vacancy precipitation nuclei does not depend critically on the choice of maximum cluster size, within the limits investigated. This is, in fact, one of the most important properties of the present model. As intimated in Sec. VI D above, an i_{max} limit is physically justified because the starting values of c_i in thermal equilibrium at T_q decrease steeply with i. At the same time it is technically desirable to work with as low an i_{max} as possible. If the result had proved dependent on the i_{max} chosen, the model would have required an extension towards bigger and bigger initial clusters. This rapidly becomes impracticable, because the computational complexity (and cost) grows extremely steeply with i. (Earlier atomistic calculations[3] were restricted to $i_{max} = 4$.)

Eventually, the gradient-controlled growth of nucleated vacancy precipitates may lead to a structure of defects, which are stable and of a size permitting observation and measurements at room temperature after the quench. This is the case for intrinsic dislocation loops in quenched aluminium, and the present calculations were numeri-

cally adjusted to that metal. The obtained concentration of nuclei corresponds to a precipitation density

$$N_i = (N_c/i)c_i \approx 10^{22}\ \mathrm{m}^{-3}. \quad (22)$$

Reported values of quench loop densities in Al vary up to 5×10^{21} m^{-3}.[11-15] The present, calculated N_i value must, however, be expected to exceed the observed loop densities for the following reasons:

(i) The model neglects all vacancy sinks other than precipitates. [In principle, this can be compensated for by introducing a "vacancy loss factor," which, however, must represent distribution inhomogeneities (cf. below).]

(ii) It is a typical feature of the observed structures of quench loops that the space distribution is strongly inhomogenous, mainly because of the action of external surfaces, grain boundaries and edge dislocation segments as vacancy sinks. Therefore, reported loop densities correspond to mean values, which are lower than local density maxima. The latter, although also subjected to some losses, would be more representative of the idealized situation of the present model.

An estimate of local loop densities from available reports[11-15] (particularly Ref. 15) gives a value

$$N_{i,\mathrm{loc}} \approx (7\pm2)\times10^{21}\ \mathrm{m}^{-3}. \quad (23)$$

Finally, it should be pointed out that the model easily can be applied to other pure metals, simply by introducing relevant numerical values of the material parameters F_1, M_1, and M_2, and of the structural parameters G_{12}, G_{21}, G_{13}, G_{31}, G_{24}, and G_{42}. The effect of alloying elements and impurities can be introduced by adding the diffusion contributions of vacancy-impurity pairs.

The present results, though numerically carried through only for aluminium, indicate that $i_{\max}$ could be restricted to 4.

ACKNOWLEDGMENTS

The authors are grateful to B. Engqvist for valuable advice in programming and to R. Österlund for extensive and skillful assistance in all the computer work.

[1]T. Federighi, in *Lattice Defects in Quenched Metals*, edited by R. M. J. Cotterill (Academic, New York, 1965), p. 217.
[2]M. Meshii in Ref. 1, p. 387.
[3]R. M. J. Cotterill, in Ref. 1, p. 97.
[4]D. Kuhlmann-Wilsdorf, in Ref. 1, p. 269.
[5]H. Doyama, in Ref. 1, p. 167.
[6]J. Silcox and M. J. Whelan, Philos. Mag. 5, 1 (1960).
[7]J. Wiberg, Y. Bergström, and O. Vingsbo, Phys. Status Soldi A 5, 677 (1971).
[8]J. S. Koehler, M. de Jong, and F. Seitz, J. Phys. Soc. Jpn. Suppl. 18, 1 (1963).
[9]A. Hellström, J. Wiberg, and R. Kalm (unpublished).
[10]J. Bass, Philos. Mag. 15, 717 (1967).
[11]P. B. Hirsch, J. Silcox, J. Smallman, and R. E. Westmacott, Philos. Mag. 3, 897 (1958).
[12]S. Yoshida, M. Kiritani, and Y. Shimomura, J. Phys. Soc. Jpn. 18, 175 (1963).
[13]G. Das and J. Washburn, Philos. Mag. 11, 955 (1965).
[14]W. J. Tunstall and P. J. Goodhew, Philos. Mag. 13, 1259 (1966).
[15]J. Wiberg and O. Vingsbo, Scand. J. Metallurgy 2, 212 (1973).